

# Study on Dynamic Wetting Behavior in Microgravity Condition Targeted for Propellant Tank

Ryoji IMAI and Mori MICHIHARA

## Abstract

Fluid behavior in microgravity ( $\mu\text{g}$ ) is different from in ground gravity since surface tension, viscous force, and wetting are dominant in  $\mu\text{g}$  condition. In propellant tank for artificial satellite and future on-orbit spacecraft, sloshing due to disturbance and settling behavior by change of acceleration have to be understood for design of propellant supply system and attitude control system. These fluid behaviors in  $\mu\text{g}$  are affected by a dynamic wetting significantly, therefore it is important to understand dynamic wetting which dominates fluid behavior. We observed fluid behaviors in cylindrical containers in microgravity conditions created by drop tower facility, and effect of viscosity and diameter of container on fluid behaviors were investigated. CFD analyses were conducted and these results were compared with experimental results. It was confirmed that numerical model considering dependence of contact line velocity in dynamic contact angle by empirical and theoretical methods provided more reasonable results.

**Keyword(s):** Microgravity, Propellant tank, Two phase flow, Surface tension, Dynamic wetting, Contact angle, CFD

Received 30 May 2017, Accepted 20 July 2017, Published 31 July 2017

## 1. Introduction

Fluid with free surface under microgravity ( $\mu\text{g}$ ) behaves differently from in ground gravity since surface tension, viscous force, and wetting are dominant in  $\mu\text{g}$  condition. Propellant tanks on liquid propellant system, e.g. attitude control system in artificial satellite, 2nd stage rocket and future on-orbit spacecraft are under  $\mu\text{g}$  condition, therefore special treatment is required for managing liquid propellant. For example, location of propellant in tank will be unstable because gravitational force is too small and its direction is indeterminate, therefore propellant management devices (PMDs) or liquid acquisition devices (LADs) are usually installed on these tanks<sup>1)</sup>. As passive methods among these devices, surface tension or capillary force is utilized to collect and acquire propellant on outlet of tank. "Gallery PMDs" are designed to make flow path to outlet wherever propellant is located<sup>1)</sup>. "Sponge PMDs" which has some thin plates called "Vaness" are designed to acquire propellant on the outlet<sup>1),2)</sup>. In order to design these PMDs, accurate estimation technology of liquid behaviors dominated by surface tension has to be established.

In the upper stages of current rocket system, operation in which engine restarts after long coasting phases is considered in order that upper stage carries the satellite near the targeted orbit so as to minimize propellant consumption for satellite thrust system<sup>3)</sup>. Propellant tanks on upper stages during coasting phase are under microgravity condition, therefore retention thrust system is installed in order to stabilize propellant location. In this system, sufficient thrust is exposed so as to settle propellant on the outlet

and to keep free surface be flatten. However if retention thrust could be reduced, propellant consumption and system weight could be minimized. However propellant behavior will be dominated by surface tension in this condition, therefore accurate estimation technology of propellant movement will provide great help for system and operation design of retention thruster.

In above mentioned situation, fluid behavior where surface tension and viscous force are governed instead of gravitational force could be simulated relatively easily. On the other hand, simulation of wetting dominating flow has much more difficulty because we have to consider both macroscopic fluid behavior and microscopic molecular phenomena in the vicinity of contact line of free surface against solid wall. In fact, there are large number of researches for dynamic wetting in ground gravity condition<sup>4),5)</sup>. However, dynamic wetting phenomena have not been fully understood since there are difficulties in treating from micro to macroscopic physics<sup>4),5)</sup>. In addition of this, these studies targeted to small scale objects such as capillary tube and droplet, therefore there are less studies treating relation between dynamic wetting and macroscopic fluid behavior under microgravity condition in which dynamic wetting is dominant even in large scale object. Additionally influence of phase change, that is, evaporation and condensation on dynamic wetting are significant especially for cryogenic fluid such as propellant and oxidizer for thrust system of spacecraft. However, this phenomena is extremely complicated since we have to treat microscopic thermal and fluid behavior including phase change.

Our final target is to understand how dynamic wetting affect macroscopic and large scale fluid behavior in closed container in

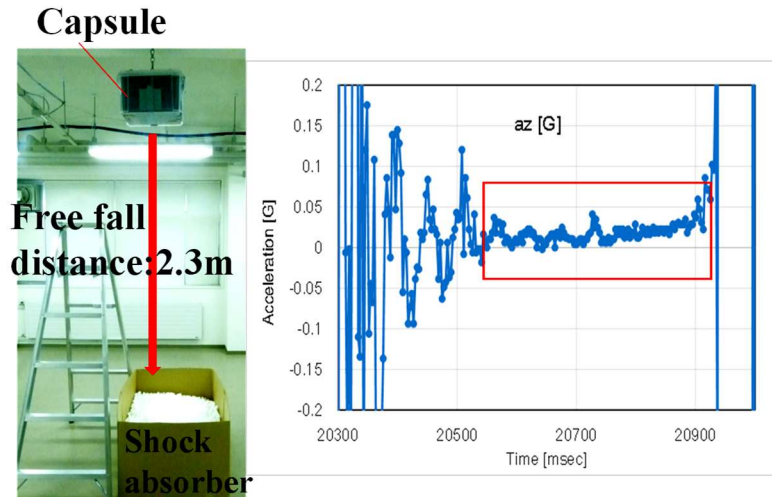


Fig. 1 Experimental apparatus for short duration microgravity condition (left) and time history of acceleration (right).

microgravity condition. Objective of present study is to investigate dynamic wetting without phase change as a first step. In this paper, results of computational fluid dynamic (CFD) analyses which investigate the effect of theoretical and empirical equations for dynamic contact angle on fluid behaviors in microgravity condition are described. Results by CFD were evaluated by experimental ones in microgravity condition obtained by free fall experimental apparatus and facility.

## 2. Method of Microgravity Experiment

We observed fluid behaviors, mainly movement of free surface in container after entering microgravity condition. Cylindrical containers with different radius and heights were selected as a test section, since symmetric two dimensional calculation domain is able to be applied.

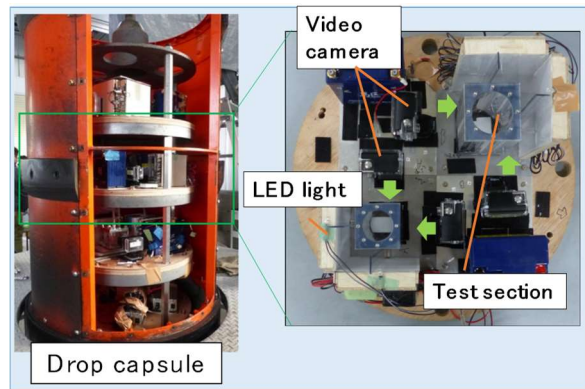
In this study, two kinds of short duration microgravity experiments were conducted. Microgravity durations were 0.4 sec and 2.5 sec obtained by 2.3 m and 45 m in free fall distance. In these experiments, silicone oil (KF-96 series by Shin-Etsu Chemical Co. Ltd.) was used as a working fluid. KF-96L-1cs and KF-96-50cs were adopted as low and high viscous fluid respectively.

### 2.1 0.4 Sec Free Fall Experimental Apparatus

Short duration microgravity condition was created by free fall apparatus shown in Fig. 1. Test section was installed on rectangular box, which we called "capsule" and capsule was placed at 2.3 m high place from ground level with hanging by a fishing line. Capsule was fallen by cutting this fishing line calmly by scissors to suppress fluctuation of acceleration by structural vibration just after starting to fall. Right figure in Fig. 1 shows time history of acceleration. We can see that order of 0.01 G in gravity level and about 0.4 sec in microgravity duration was performed.

### 2.2 2.5 Sec Free Fall Experimental Facility

Short duration microgravity condition was created by free fall facility named by COSMOTORRE in Uematsu Electric Co., Ltd. General description of this experimental apparatus is shown in Fig. 2. Test section was installed on cylindrical drop capsule prepared by Uematsu Electric Co., Ltd. This capsule is hung up



Left: Experimental apparatus installed on drop capsule. Right: Test section and observation system.



Test Section

Test section :  
 Material: acrylic resin  
 Dia.: 30,45,60 mm  
 Height: 60,90,120 mm

Fig. 2 Experimental apparatus and test section.

by crane and raised at about 50 m high before dropping. Free fall distance of capsule is 45 m, and microgravity duration is obtained to be about 2.5 sec. Experimental rack which installs experimental apparatus is being floated in the capsule during free falling, therefore high quality microgravity condition is obtained. Microgravity level in our experiments was performed to be order of 0.001 G. On upper side in **Fig. 2**, experimental apparatus in this experiment is shown. Two sets of cylindrical containers as test section, video camera (GoPro Hero4), LED light source and battery were installed on wooden circular plate. Fluid behaviors in each test section were observed from two direction, therefore four sets of video cameras were used. Test section is shown on the lower side of **Fig. 2**. Test section is made of transparent acrylic resin, and cylindrical shape is formed on the rectangular block, which intends to minimize the effect of refraction in observing liquid behavior in container. Three kinds of test section were prepared; 30, 45, and 60 mm in diameter and 60, 90, and 120 mm in height respectively. The objective to prepare these test sections are to clarify the effect of scale on unstable fluid behavior in sudden change of gravitational force. Scale will be related to inertia force, capillary force, viscous force and gravitational force. However main subjects of this paper are comparison between experimental and numerical results and treatment of dynamic contact angle. Therefore description of discussion about scale effect as well as results for 45 mm in diameter and 90 mm in height won't be described in this paper.

This experimental apparatus was installed on third stage from bottom of experimental rack shown as **Fig. 2**.

### 3. Method of Numerical Calculation

Fluid behaviors in cylindrical container under microgravity condition in consideration of dynamic wetting were analyzed by commercial CFD code of ANSYS FLUENT ver. 15.

#### 3.1 Calculation Domain

**Figure 3** shows calculation domain. Flow field was assumed to be two dimensional axisymmetric, therefore calculation domain was set to be rectangular region. In the microgravity experiments, it was confirmed that free surface behaved two-dimensionally by the observations from two direction. Therefore two dimensional calculation domain in this study is reasonable. Then, meshes were set to be finer approaching to the solid wall. Number of cells in calculation domain is 3600 for domain corresponding to each test section. Therefore averaged cell size increases with domain size. This fact doesn't affect quality of numerical results since microscopic region in the vicinity of contact line is excluded from calculation domain by introducing treatment of dynamic wetting mentioned hereafter.

VOF (Volume of Fluid) method was employed to calculate two phase flow, and geometric reconstruction scheme<sup>6)</sup> was applied as an interface reconstruction algorithm. Liquid and gas flow

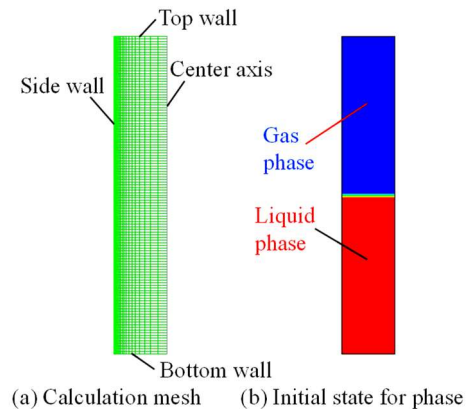


**Fig. 3** Calculation domain.

**Table 1** Fluid substance and these properties in present calculation.

Fluid		Dynamic viscosity [mm <sup>2</sup> /s]	Density [kg/m <sup>3</sup> ]	Surface tension [mN/m]
Liquid phase	KF-96L-1cs	1.0	816.6	17
	KF-96-50cs	50.0	957	20.8
Gas phase	Air	14.6	1.225	N/A

were assumed to be laminar. Surface tension was considered as a source term in momentum equations by CSF (Continuum Surface Force) method<sup>7)</sup>.

Diameter and height of calculation domain was 30,45,60 mm and 60,90,120 mm respectively corresponding to test section. As an initial condition, volume of liquid was given to be a half of container volume. **Table 1** shows fluids substance and these properties in present calculation.

#### 3.2 Treatment of Dynamic Wetting

In the vicinity of contact line, that is, intersection of free surface and solid wall, thin liquid film is formed. It is difficult to simulate flow field in this region reasonably since molecular force is not able to be neglected. Additionally some treatments have to be required to prevent numerical instability by applying extremely fine mesh in thin liquid film region. To overcome this difficulty, a method of introducing dynamic contact angle and applying this as a boundary condition on solid wall is generally taken. In present study, existing equations for dynamic contact angle with dependence of contact line velocity was applied as a boundary condition on solid wall. As another method, flow field in thin liquid film region was separately calculated, where effect of molecular force was considered, and dynamic contact angle with dependency of contact line velocity was obtained as a numerical results. We call this method as "thin liquid film theory".

### A. Method to use Existing Equations for Dynamic Contact angle

There are many equations for dynamic contact angle which has dependency of contact line velocity by theoretical and empirical approach. Cox's<sup>8)</sup> and Katoh's<sup>9),10)</sup> equations were used to provide dynamic contact angle. These equations are shown as follows;

Cox's equation

$$\theta_d = (\theta^3 + 9C \cdot Ca)^{1/3}, C = \ln(L/S) \quad (1)$$

Katoh's equation

$$|\cos\theta_d - \cos\theta| = \frac{3(1-\varepsilon)}{\varepsilon \tan\theta_d} Ca \quad (2)$$

where  $\theta$  is static contact angle,  $\theta_d$  dynamic contact angle,  $L$  characteristic length,  $S$  slip length, and  $\varepsilon$  the ratio of the surface area occupied by defects.  $Ca$  is a dimensionless parameter of Capillary number defined as;

$$Ca = \frac{\mu U}{\sigma} \quad (3)$$

where  $\mu$  is viscosity,  $U$  contact line velocity, and  $\sigma$  surface tension.

Cox tried to represent flow in the vicinity of contact line analytically, then he found that viscous stress on contact line had singularity, that is, integral of this stress became infinite<sup>8)</sup>. Therefore he introduced slip length  $S$ , the area length from contact line in which shearing stress on solid wasn't considered. From the Brake's review<sup>5)</sup> it is mentioned that  $S$  has very wide value according to liquid substance and experimental conditions, therefore, this has to be treated as adjustable parameter. In our calculation,  $C$  parameter was treated as adjustable parameter since  $S$  is included in the definition formula of  $C$ .

In Katoh's equation,  $\varepsilon$  is the ratio of the surface area occupied by defects. Here, defects means roughness or absorbed foreign molecules with a macroscopic scale on the solid surface. Additionally,  $\varepsilon$  is treated as adjustable parameter<sup>10)</sup>.

Contact line velocity was obtained by multiplying velocity vector on numerical cell neighbored on sidewall and unit gradient vector of volume fraction of liquid.

### B. Method to Consider a Thin Liquid Film Flow Theory near Contact Line

In order to consider a thin liquid film flow near contact line, disjoining pressure as well as surface tension were introduced to consider pressure difference through free surface. **Figure 4** shows thin liquid film flow and pressure difference through free surface<sup>11),12)</sup>. Thickness of liquid film is expressed by  $h(x)$  as a function of coordinate  $x$  along solid wall.

We constructed governing equations for thin liquid film theory by combining methods by Standingford<sup>11)</sup> and Wang<sup>12)</sup>. Pressure balance through free surface is show as follows;

$$p_g = p_l + p_c + p_d \quad (4)$$

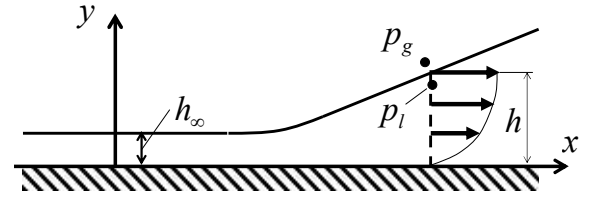


Fig. 4 Thin liquid film flow near contact line.

where  $p_g$  is gas phase pressure,  $p_l$  liquid phase pressure.  $p_c$  capillary pressure difference, and  $p_d$  disjoining pressure<sup>12),13)</sup> is given as follows;

$$p_c = \sigma \kappa \quad (5)$$

$$p_d = \frac{B}{h^4} \quad (6)$$

where  $\kappa$  is curvature of free surface,  $B$  is coefficient for disjoining pressure expressed by following equation;

$$\kappa = \frac{h_{xx}}{(1+h_x^2)^{1.5}} \quad (7)$$

where subscript  $x$  indicate differential of  $x$  respectively.

Disjoining pressure is introduced to consider the effect of molecular force in the vicinity of contact line. Equation for disjoining pressure is derived by exchanging molecular force obtained from Lenard-Jones potential to pressure, then this is shows as follows<sup>14)</sup>;

$$p_d = \frac{A}{h^3} \quad (8)$$

The coefficient "A" is called as Hamaker constant<sup>14)</sup>.

In numerical analysis of thermal and fluid behavior for evaporating menisci, Panchamgam et. al. employed eq.(6) as disjoining pressure for relatively thicker liquid film. We tried both equations, consequently it was confirmed that reasonable results were obtained in eq.(6). Therefore, we applied eq.(6) as disjoining pressure hereafter.

If we consider  $p_g = 0$  as a base pressure,  $p_l$  is replaced by  $p$ ,

$$p = -p_c - p_d = -\sigma \kappa - \frac{B}{h^4} \quad (9)$$

From the lubrication theory<sup>15)</sup>, following equation is derived;

$$u_{yy} = \frac{p_x}{\mu} \quad (10)$$

where subscript  $y$  indicate differential of  $y$  respectively.

From the continuous condition for volumetric flow rate and solution of eq.(10), we obtain;

$$-p_x = 3\mu U \frac{h-h_\infty}{h^3} \quad (11)$$

where  $h_\infty$  is coating thickness shown in **Fig. 4**.

From eq.(9) to eq.(11), following ordinary differential equation

for thickness of liquid film  $h(x)$  is derived;

$$h_{xxx} = \frac{3\mu U}{\sigma} \frac{h-h_\infty}{h^3} (1+h_x^2)^{3/2} + \frac{3h_x}{h_x^2+1} h_{xx}^2 + \frac{4B}{\sigma} \frac{1}{h^5} h_x (1+h_x^2)^{3/2} \quad (12)$$

In order to solve this differential equation, coating thickness  $h_\infty$  has to be provided. This thickness is supposed to be corresponding to so-called “precursor film” which is extremely difficult to be observed. In our study, this thickness was treated as adjustable parameter, and was determined to be  $4.0 \times 10^{-8}$  m, in which it was confirmed that reasonable relationship between contact line velocity and dynamic contact angle was obtained as a result of parametric study of  $h_\infty$ . However more reasonable method to determine  $h_\infty$  has to be considered, this is currently open problem. In this numerical analysis, liquid behavior in microgravity condition created drop tower facility was targeted. Therefore consideration of coating film or precursor film is supposed to be reasonable in this calculation since solid wall faced on gas phase will be wet due to swinging motion of experimental apparatus during preparation phase of microgravity experiment.

It was shown that curvature of liquid film surface obtained by eq.(12) approached to constant value, where we defined dynamic contact angle from a gradient of thickness of liquid film. Relationships between contact line velocity and dynamic contact angle was calculated, which were inputted to CFD calculation model as boundary condition at side wall.

### 4. Results of Microgravity

#### 4.1 Results by 0.4 Sec Fall Experimental Apparatus

Figure 5 shows dynamic liquid behavior in cylindrical container with 30 mm in diameter and 60 mm in height. Here dynamic viscosity of liquid was  $1 \text{ mm}^2/\text{s}$ . From this figure, we can see that contact line of free surface against solid wall was raised by surface tension and that free surface on center axis went down. Also we can see that curvature of free surface on center line was larger just after entering microgravity condition, then became smaller and free surface on center line went up.

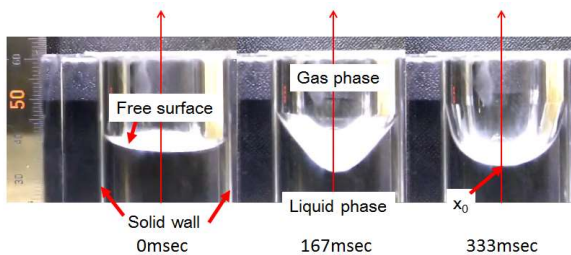


Fig. 5 Dynamic behavior of liquid in container. 30 mm in diameter and 60 mm in height. Dynamic viscosity is  $1 \text{ mm}^2/\text{s}$ .

#### 4.2 Results by 2.5 Sec Free Fall Experimental Facility

Figure 6 shows dynamic liquid behavior in cylindrical container with 30 mm in diameter and 60 mm in height, same size as one used in 0.4 sec free fall experimental apparatus. From this figure, we can see that fluid behavior just after entering microgravity condition was similar with one by 0.4 sec free fall experimental apparatus. During microgravity condition obtained in this free fall facility, movement of free surface almost ceased,

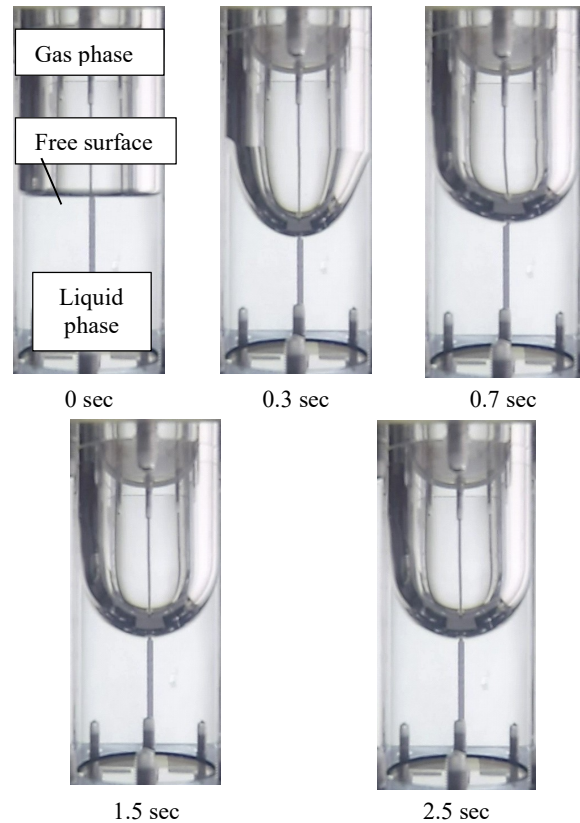


Fig. 6 Snapshot of liquid behavior. Diameter is 30 mm and height is 60 mm. Dynamic viscosity is  $1 \text{ mm}^2/\text{s}$ .

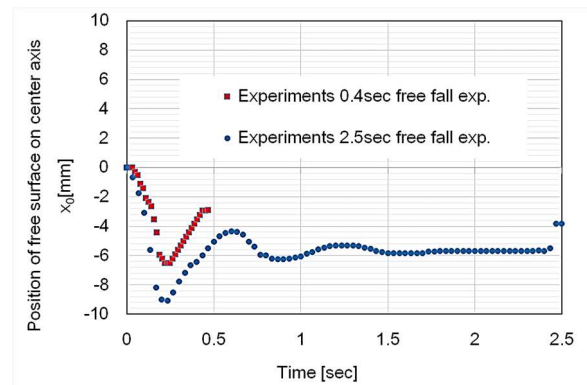
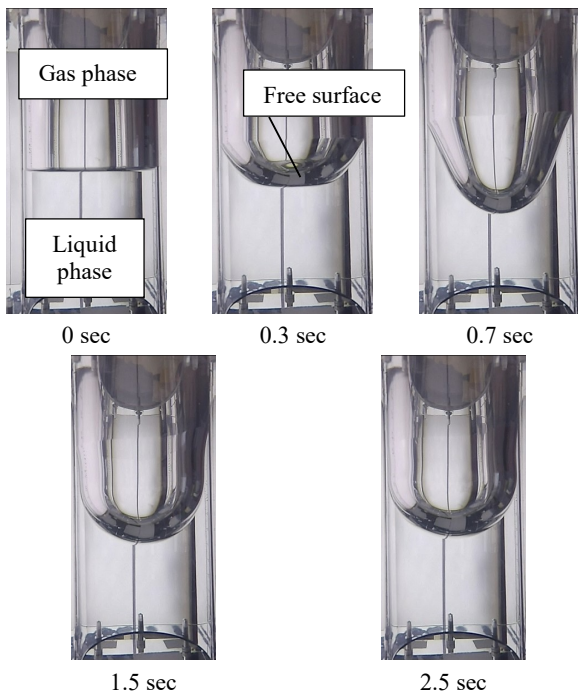


Fig. 7 Time history of position of free surface on center axis.



**Fig. 8** Snapshot of liquid behavior. Diameter is 60 mm and height is 120 mm. Dynamic viscosity is 1 mm<sup>2</sup>/s.

that is, fluid behavior reached almost stable. We can see that curvature of free surface was almost uniform, therefore, shape of free surface was similar with part of sphere.

**Figure 7** shows the time history of position of free surface on center axis obtained by 0.4 sec free fall apparatus and 2.5 sec free fall facility. We can see that coordinate of free surface on center axis went down to negative coordinate just after entering microgravity condition and went up after reaching minimum coordinate. It is found that this minimum value was smaller in experiment by 2.5 sec free fall facility, since microgravity level is lower than by 0.4 sec free fall apparatus, therefore contact line of free surface was raised larger.

**Figures 8 and 9** show dynamic liquid behavior of 1 mm<sup>2</sup>/s and 50 mm<sup>2</sup>/s in dynamic viscosity for 60 mm in diameter and 120 mm in height. In **Fig. 8**, we can see flatten shape at 0.3 sec and larger curvature at 0.7 sec in free surface before reaching stable and uniform curvature. In **Fig. 9**, we can see that free surface approaches to stable shape without overshoot seen in case of low viscosity.

### 4.3 Measurement of dynamic contact angle

In order to obtain the relation between contact line velocity and dynamic contact angle, we captured image where contact line was enlarged by digital video camera. These measurements were conducted in both 0.4 sec free fall experiment and 2.5 sec free fall experiment respectively. As for 0.4 sec free fall experiment, measurement method and results were described in previous

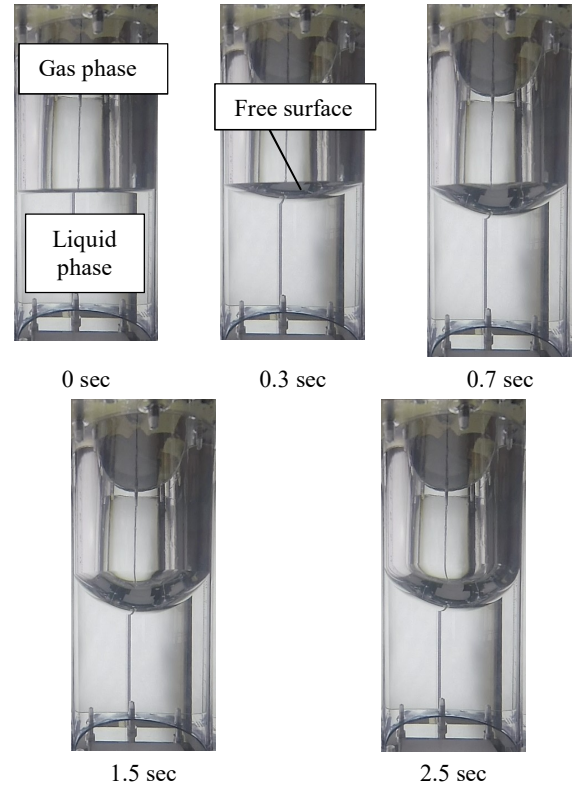


**Fig. 9** Snapshot of liquid behavior. Diameter is 60 mm and height is 120 mm. Dynamic viscosity is 50 mm<sup>2</sup>/s.

paper by authors<sup>16)</sup>, therefore detail description will be skipped.

We compared our experimental results with ones by Cox's formula, consequently, it was found that dynamic contact angle with range of 5 to 40 in 'C' value can generally cover our experimental results.

Measurements and adjustment in C value in 2.5 sec free fall experiment is described below in detail. **Figure 10** shows the snapshot of liquid behavior in container of 60 mm in diameter. Location of contact line and contact angle were measured by use of image processing software named "ImageJ". A contact line speed was calculated from time derivative of contact line coordinate. **Figure 11** shows contact line velocity vs. dynamic contact angle obtained from experimental results shown in **Fig. 10**.

In this figure, advanced dynamic contact angle was indicated since contact line proceeded upward. Dynamic contact angle by Cox' equation with various coefficient 'C' values was also shown in this figure. We can see that there are some scattering in experimental data. There were some errors in detecting contact point due to insufficient resolution in image and due to lack of performance of video camera. We expect this scattering will be reduced if we capture further enlarged image of free surface near contact line. Anyway we can see that dynamic contact angle by Cox's equation with range of 1 to 5 in 'C' value can generally cover our experimental results.

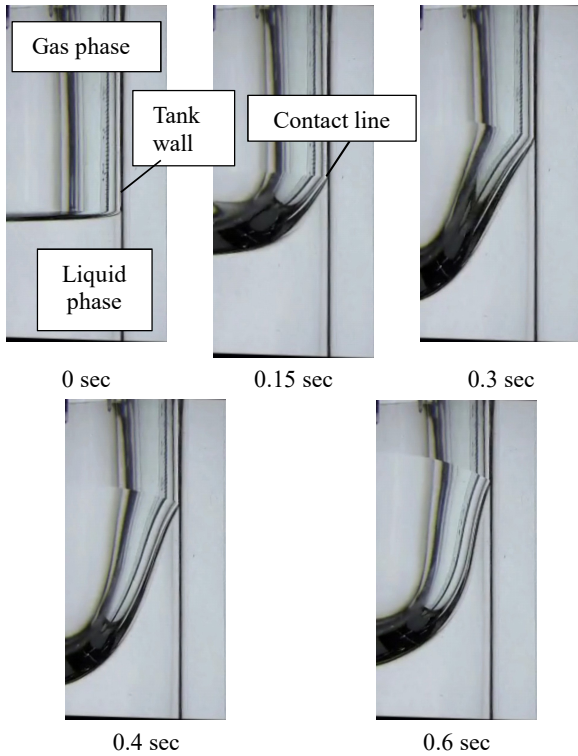


**Fig. 10** Snapshot of free surface shape near contact line. Diameter is 60 mm and height is 120 mm. Dynamic viscosity is 1 mm<sup>2</sup>/s.

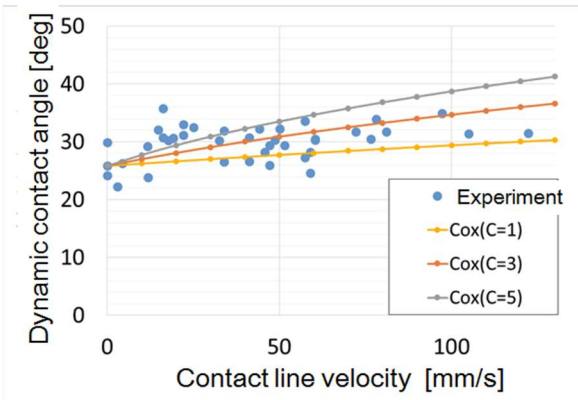


**Fig. 11** Contact line velocity vs. dynamic contact angle.

### 5. Results of numerical calculations

We calculated unsteady fluid behavior in cylindrical container when acceleration was imposed vertically downward changed from 1 G to 0.01 G and 0.001 G in order to simulate microgravity condition by free fall experiment. These conditions correspond to results by 0.4 sec free fall experimental apparatus and 2.5 sec free fall experimental facility respectively.

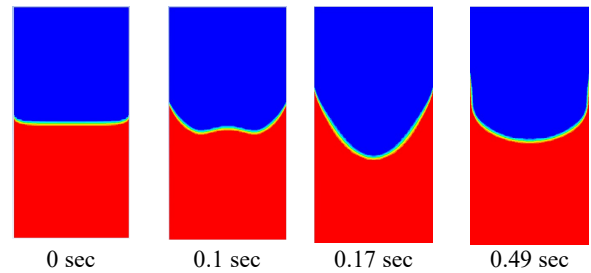


**Fig. 12** Snapshot of liquid behavior. Dynamic contact angle is 4.0 deg. Red and blue portion indicates liquid and gas phase respectively. Diameter of container is 30 mm and height is 60 mm. Dynamic viscosity is 1 mm<sup>2</sup>/s.

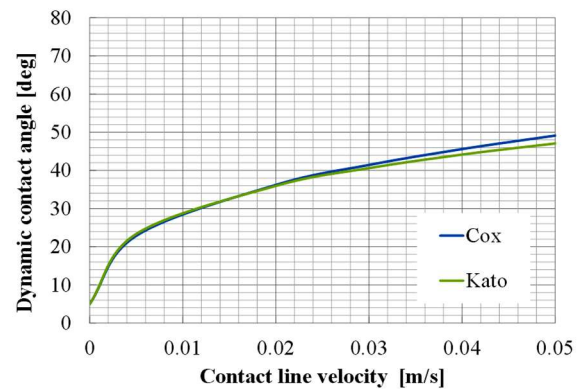
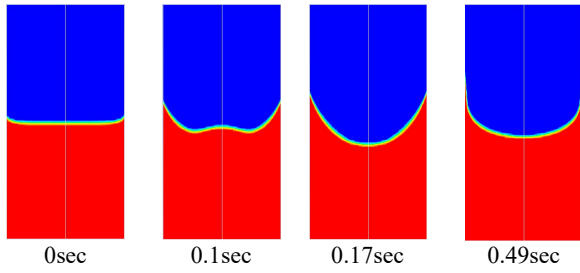


**Fig. 13** Contact line velocity vs. dynamic contact angle by Cox's and Kato's equation

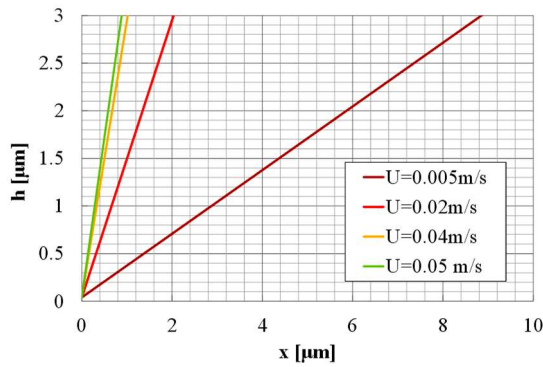
#### 5.1 Numerical results corresponding to experiment by 0.4sec free fall experimental apparatus

Figure 12 shows snapshot for contour of volume fraction in liquid phase where dynamic contact angle was given to be constant value of 4.0 deg which was obtained from observation of static meniscus for 30 mm in diameter of container. Red and blue portion shows the area where volume fraction of liquid is unity and zero respectively. This means that red and blue portion indicate liquid and gas phase respectively. From these figures, we can see that free surface was raised by surface tension on the side wall, and concave shape in free surface is formed between side wall and center axis and convex shape on center axis just after entering to microgravity condition. Then this concave shape disappeared by free surface on the center axis starting to go down. After this, contact line on side wall repeated downward and upward movement, and free surface on center axis repeated opposite direction movement simultaneously. This repeatedly movement would damp by viscous stress.

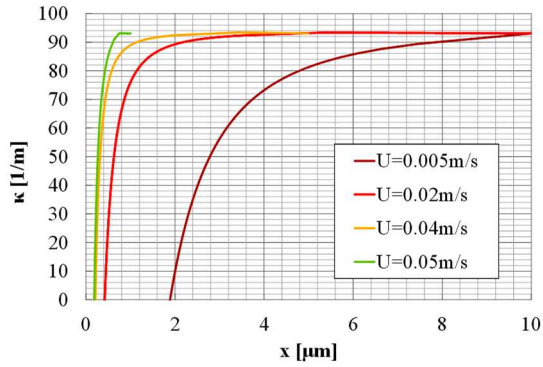
We calculated liquid behaviors where Cox's and Kato's equation was applied as dynamic contact angle. Prior to conduct this calculation, we obtained relation between contact line velocity and dynamic contact angle shown as Fig. 13. Here, C in



**Fig. 14** Snapshot of liquid behavior. Dynamic contact angle was given by Cox’s equation. Coefficient C is 29.8. Red and blue portion indicates liquid and gas phase respectively. Dynamic viscosity is  $1 \text{ mm}^2/\text{s}$ .



(a) Thickness of liquid film



(b) Curvature of liquid film

**Fig. 15** Thickness and curvature of liquid film.

Cox formula is 29.8, and  $\varepsilon$  in Kato’s formula is 0.021, these value were same as ones used in Kato’s experiment<sup>10</sup>. We can see that results by Cox’s and Kato’s equation agree with each other.

**Figure 14** shows snapshot of liquid behavior where Cox’s equation was applied as dynamic contact angle with dependence of contact line speed. There are a less difference in history of free surface shape compared to constant dynamic contact angle of  $\theta_d = 4 \text{ deg}$ . Also we confirmed that effect of C on history of free surface shape was very small with range of 5 to 40 in C. In

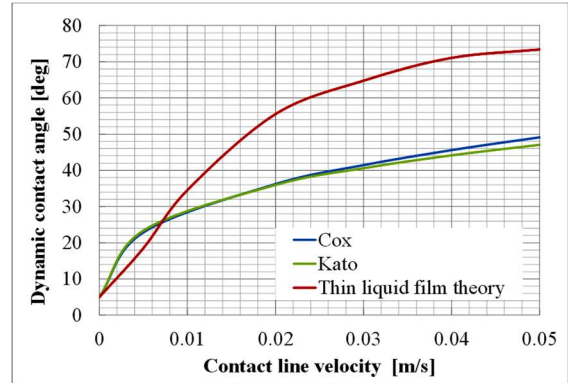


**Fig. 16** Contact line velocity vs. dynamic contact angle considering thin liquid film theory.

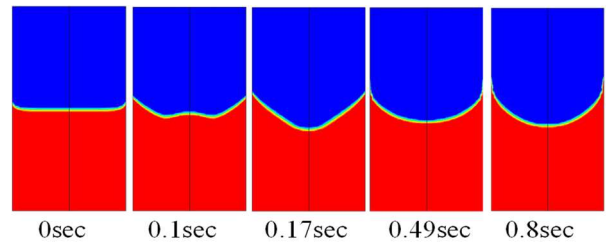


**Fig. 17** Snapshot of liquid behavior Dynamic contact angle was applied according to thin liquid film theory. Red and blue portion indicates liquid and gas phase respectively. Dynamic viscosity is  $1 \text{ mm}^2/\text{s}$ .

addition of this, we investigated dynamic liquid behavior by using Kato’s equation as dynamic contact angle. We confirmed that this results were consistent with ones by giving constant value and variable value according to Cox’s equation in dynamic contact angle.

Next we will show calculated results which considered flow in the vicinity of contact line. As a first step, we obtained relationship between contact line speed and dynamic contact angle. **Figure 15** shows  $h(x)$ ; distribution of liquid film and curvature of free surface obtained as solution of eq.(10). Here, coefficient for disjoining pressure was set to be  $B = -1.2 \times 10^{-27}$  used by Panchamgam et al.<sup>13</sup> The effect of contact line speed  $U$  was also shown in these figures. We can see that curvature converged as distance from contact point  $x$  increased. Dynamic contact angle was obtained from the gradient of liquid film thickness at which curvature converged.

**Figure 16** shows relationship between contact line velocity and dynamic contact angle obtained by solving eq. (10). In this figure, results using Cox’s and Kato’s equation were also shown. We can find that dynamic contact angle by thin liquid film theory was much larger than by other equations. We made a polynomial equation for contact line velocity vs. dynamic contact angle. This equation for dynamic contact angle was applied as boundary condition on side wall in the numerical calculations.

Figure 17 shows snapshot of liquid behavior when dynamic contact angle with dependence of contact line velocity. We can see that rising distance of contact line is smaller compared with results in constant value of 4 deg and Cox's equation in contact angle shown in Figs. 12 and Fig.14.

**5.2 Numerical Results Corresponding to Experiment by 2.5 Sec Free Fall Experimental Facility**

Figures 18 and 19 show snapshot of volume fraction of liquid phase in case that dynamic contact angle was given to be constant

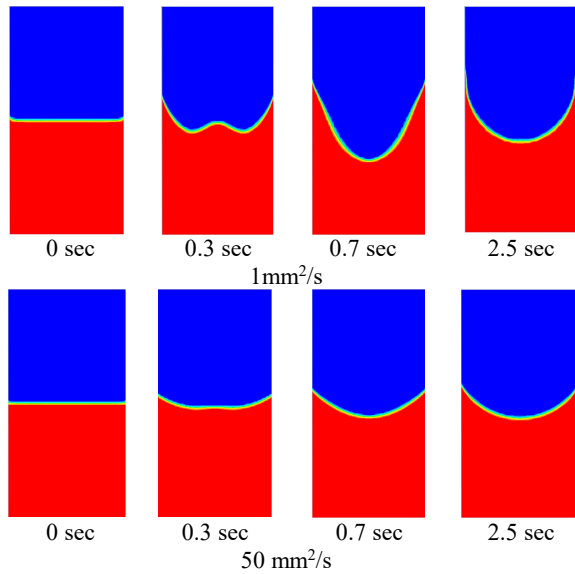


Fig.18 Snapshot of liquid behavior. Dynamic contact angle is 4.0 deg. Red and blue portion indicates liquid and gas phase respectively. Diameter is 60 mm and height is 120 mm.

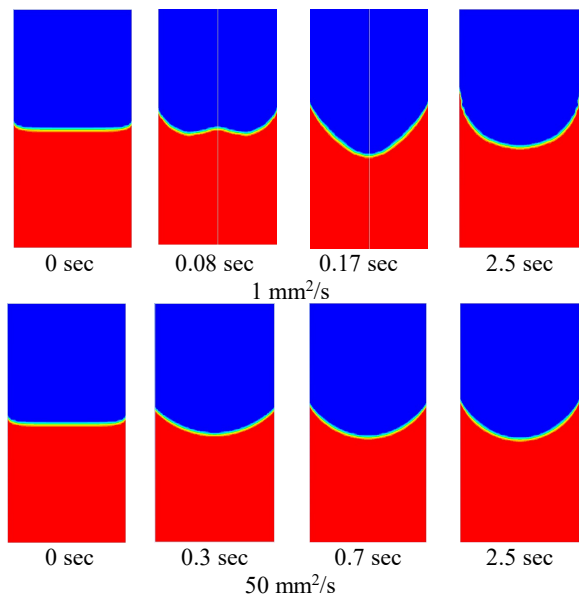


Fig. 19 Snapshot of liquid behavior. Dynamic contact angle is 4.0 deg. Red and blue portion indicates liquid and gas phase respectively. Diameter is 30 mm and height is 60 mm.

value which was obtained from observation of static meniscus for 60 mm and 30 mm in diameter of container. In low viscosity case, liquid behavior is similar with one obtained in the condition for 0.4 sec free fall experimental apparatus. In high viscous liquid, we can't see convex shape and going down movement for free surface on center axis, and we can see that displacement of free surface is much smaller than for low viscous liquid. In low viscosity case for 30 and 60 mm in diameter, we can see concave shape in free surface on center axis, and it takes longer time in φ60 mm case to obtain that shape from entering micro gravity condition. This means liquid moves slower in larger diameter of container.

We calculated fluid behaviors in case that dynamic contact angle was given by Cox's formula and thin liquid films theory for 60 mm and 30 mm in diameter of container respectively. We confirmed that liquid behaviors were quite similar with ones in constant dynamic contact angle, therefore we skip snapshot of liquid behavior in these cases.

**5. Discussion**

**5.1 Comparison between Experimental and Numerical results for 0.4 Sec Free Fall Experimental Apparatus**

Time history of center position was compared between numerical and experimental results. Figure 20 shows comparison between experimental and numerical results where Cox's equation was applied as dynamic contact angle. We can see that center position on center line went down just after microgravity condition started, then went up. Also we can see that the dependency of coefficient 'C' is very small in numerical results. It was found that agreement between experimental and numerical results was not so good especially after about 0.2 sec. In Fig. 20 we can see some fluctuations in numerical results. These phenomena were also seen in other low viscous fluid cases mentioned hereafter, however, these were not obtained in experimental results. We supposed that these fluctuations were caused by numerical error, which was expected be reduced by appropriate surface capturing algorithm. This is currently open problem.

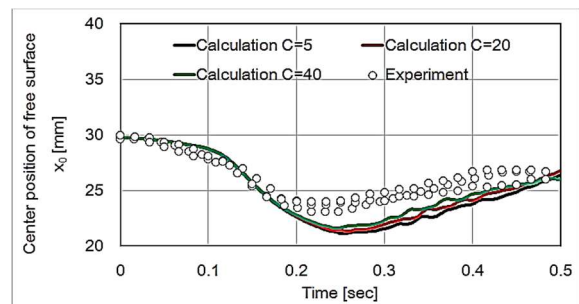
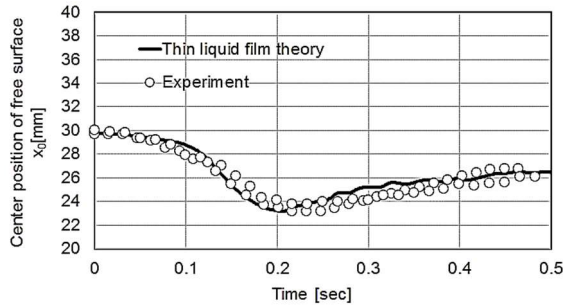


Fig. 20 Time history of center position of free surface (Comparison with Cox's equation).



**Fig. 21** Time history of center position of free surface (Comparison with thin liquid film theory).

**Figure 21** shows comparison between experimental and numerical results where dynamic contact angle was obtained by thin liquid film theory. It was found that numerical results agreed with experimental one very well.

### 5.2 Comparison between Experimental and Numerical Results for 2.5 Sec Free Fall Experimental Facility

**Figures 22 and 23** shows the history of center position and contact point against solid wall in free surface, and comparison between experimental and numerical results where constant value, Cox’s equation, and thin liquid film theory were applied as dynamic contact angle in  $\phi 60$  mm container, and low and high viscous case respectively. We can see experimental results shows that center position on center axis went down just after microgravity condition started, then went up. However in case of low viscous liquid in  $\phi 60$  mm container, numerical results show that change in position of free surface on center axis is very small just after entering microgravity condition, therefore there is disagreement between experimental and numerical results. On the other hand, we can’t see this disagreement in other cases shown in **Fig 23**. This disagreement results from the fact that concave shape of free surface on the center axis couldn’t be detected due to measurement method in the experiments.

We can see that numerical results concerning position of free surface on side wall with constant contact angle don’t agree with experimental ones in low viscous liquid, that is, contact position by numerical results decreased faster after about 1.5 sec. On the other hand, it is found that numerical results by Cox formula and thin liquid film theory agree with experimental ones favorably.

**Figure 24** shows experimental and numerical results in case of low viscous liquid in  $\phi 30$  mm container. We can see that agreements between experimental and numerical results were favorable in the history of free surface position on center axis. And it is found that numerical results concerning position of free surface on side wall with constant contact angle don’t agree with experimental ones in low viscous liquid. On the other hand, we can see that numerical results by Cox formula and thin liquid film theory agrees with experimental ones very well.

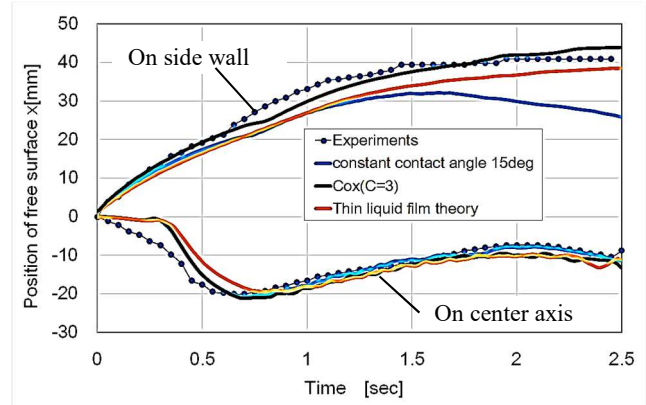


**Fig. 22** Contact line velocity vs. dynamic contact angle. Dia.:60 mm, height:120 mm, low viscous liquid case (KF-96L-1cs).

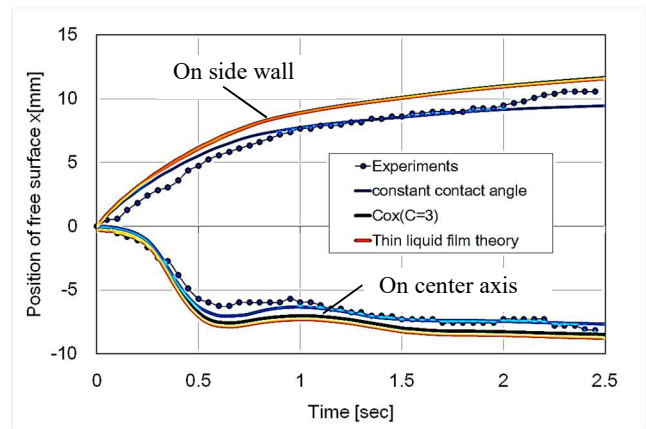


**Fig. 23** Contact line velocity vs. dynamic contact angle. Dia.:60 mm, height:120 mm, high viscosity liquid case (KF-96L-50cs).

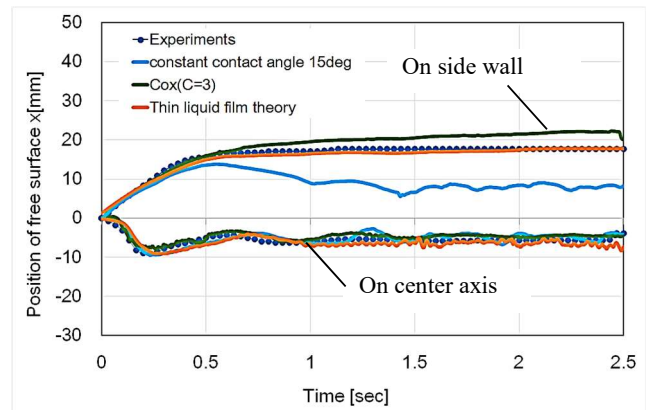


**Fig. 24** Contact line velocity vs. dynamic contact angle. Dia.:30 mm, height:60 mm, low viscosity liquid case (KF-96L-1cs).

## 6. Conclusion

Numerical calculation for dynamic wetting behavior in cylindrical container was conducted, and these results were evaluated by short duration microgravity experiments using 0.4 sec free fall experimental apparatus and 2.5 sec free fall

experimental facility.

In numerical calculations, dynamic contact angle with dependency of contact line velocity was adapted as the boundary condition on side wall. Relation between contact line velocity and dynamic contact angle was obtained in advance by two kinds of method; Cox's equation and thin liquid film theory. Dynamic liquid behaviors after entering to microgravity condition were investigated in detail.

Dynamic wetting behaviors in microgravity conditions were observed by using short duration free fall apparatus. Evaluation of numerical results were made by comparing with experimental results. In case of microgravity condition by 0.4 sec free fall experimental apparatus, it was shown that numerical result where dynamic contact angle was calculated by thin liquid film theory agreed with experimental ones using better than by Cox's formula and by given as constant value. In case of microgravity condition by 2.5 sec free fall experimental facility, we found that numerical results by Cox's formula and thin liquid film theory agreed with experimental ones very well.

Finally, we have to evaluate numerical model by more experimental data in microgravity condition. As a final target, we are going to construct the numerical calculation model considering microscopic wetting phenomena, macroscopic fluid behavior, and their interrelationship. Also dynamic wetting with phase change through free surface has to be investigated targeted to cryogenic propellant management system for future on-orbit transfer vehicle.

## References

- 1) F.T. Dodge: The New "Dynamic Behavior of Liquids in Moving Containers"  
ftp://apollo.ssl.berkeley.edu/pub/ME\_Archives/Government%20and%20Industry%20Standards/NASA%20Documents/SwRI\_Fuel\_Slosh\_Update.pdf (2014).
- 2) R. Imai, Y. Takano, K. Yamada, K. Hama and S. Nakamura: Proceedings of the Twenty-Fifth International Symposium on Space Technology and Science selected papers Kanazawa, ISTS 2006-a-02, **25** (2006) 1.
- 3) M. Niitsu, M. Yasui, K. Shimura, J. Yabana, Y. Tanabe and K. Ishikawa: Mitsubishi Heavy Industries Technical Review, **51** (2014) 26.
- 4) D. Bonn, J. Eggers, J. Indekeu, J. Meunier and E. Rolleyonn: Review of modern physics, **81** (2009) 739.
- 5) T.D. Blake: J. of Colloid and Interface Science, **299** (2006) 1.
- 6) D.L. Youngs: Numerical Methods for Fluid Dynamics, Academic Press (1982).
- 7) J.U. Brackbill, D.B. Kothe and C., Zemach: J. of Computational Physics, **100** (1992) 335.
- 8) R. Cox: J. of Fluid Mechanics, **168**, (1986)169.
- 9) K. Katoh, T. Wakimoto and S. Nitta: J. Jap. Soc. Exp. Mech. 10, s62-s66 (2010).
- 10) L. Katoh, T. Wakimoto, Y. Yamamoto and T. Ito: Experimental Thermal and Fluid Science, **60** (2015) 354.
- 11) D.W.F. Standingford and L.W. Schwartz: AIAA, 99-1035 (1999).
- 12) H. Wang, J.Y. Murthy, and S.V. Garimella: Int. J. of Heat and Mass Transfer, **51** (2008) 3007.
- 13) S.S. Panchangam, S.J. Gokhale, J.L. Plawsky, S. DasGupta and P.C. Wayner, Jr.: Trans ASME, J. of Heat Transfer, **127** (2005) 231.
- 14) S. Batzdorf: Technische Universit Darmstadt Ph D Thesis, 2015.
- 15) F.P. Bretherton: J. of Fluid Mechanics, p. 166 (1960).
- 16) R. Imai, Y. Amanom and S. Goto: proceeding of AJCPP2016, (2016).